Evaluating the effective thermal conductivity of cement mortar through x-ray scanning

Iman Asadi [a], Guomin Ji [b],[*], Mohammad Hajmohammadian Baghban [b],[**]

[a] Department of Structural Engineering, Norwegian University of Science and Technology, NO-7491, Trondheim, Norway
[b] Department of Manufacturing and Civil Engineering, Norwegian University of Science and Technology, Gjøvik, Norway

A R T I C L E I N F O

A B S T R A C T

The effective thermal conductivity of cement mortar as a porous material depends on its solid phase and void phase conductivity. Therefore, a sample's pore distribution can highly impact the value of effective thermal conductivity. For this reason, an x-ray CT scanner was applied to detect air-void content in mortars with different mix proportions. After 28 days of curing, the thermal conductivity of samples ($40 \times 40 \times 80$ mm^3) was measured by the transient plane source (TPS) apparatus, TPS2500. Then, the samples were scanned by a Zeiss Metrotom 1500 CT scanner to detect the macro pore content. Finally, the VGStudio Max 3.0 software was applied to observe the voids and simulate the effective thermal conductivity. The results showed that the total macro void contents (in this study, voids bigger than 52 μm) were increased up to 15% and 33% for samples with the cement the sand ratio of 1:3 and 1:4 compared to the sample with the c:s ratio of 1:2. However, the results indicated that the void fraction is not uniform. Therefore, effective thermal conductivity can vary in different sample locations. The finding shows that x-ray scanning and image analysis is the proper method to precisely determine the effective thermal conductivity of cement-based materials.

1. Introduction

Cement mortar is a composite material composed of cement (hydraulic binder), sand (as fine aggregate), water, and additive in some cases. Cement mortar can be used widely for pavement-smoothing, rendering, masonry bedding, and joint glue [1–3]. Recently, more researchers and industrial producers have focused on insulating cement-based materials to reduce the cost of energy and greenhouse gas emissions and increase thermal comfort [4–6]. The amount of heat transfer through the walls is directly related to the thermal conductivity of its component like concrete and mortar [7]. BS EN 998- 1 [8] defined the "thermal insulating mortar" as a mortar with a thermal conductivity lower than 0.2 W/m.K.

The heat transfer in porous materials like cement mortar is complicated due to the irregularity of microstructures [9]. Conduction is the main mean of heat transfer in both the solid and gas phase of mortar and concrete. It is known that the convective heat transfer can be ignored for (Gr.Pr) $< 10^3$ and becomes more significant for voids larger than 1 cm at a temperature above 200 °C [10,11]. Furthermore, the thermal behavior of mortar and concrete affects its fire resistance ability [12]. The thermal characteristic of mortar and concrete is related to the w/b ratio, c/s ratio, thermal properties of raw materials used as binder and aggregate, etc. [13–15]. Also, cement paste, mortar, and concrete are heterogeneous materials, and their conductivity is related to the microstructures [16].

It is known that thermal conductivity is an intensive property, and it can vary in different materials places. Usually, the thermal conductivity of concrete is determined by experimental measurement, numerical simulation, or prediction models. Prediction models and numerical simulation are helpful methods to avoid costly and complex measurement methods [17,18]. Several studies indicated that the thermal conductivity of cement-based materials is related to the pore structure [19–22] and can be predicted by assuming a two-phase material, i.e., solid phase and void phase [23–27]. Also, different models were proposed to estimate the effective thermal conductivity based on the thermal conductivity and the volume of the solid and gas phases [28–32].

The common models for effective thermal conductivity are the series, parallel, Maxwell, and effective medium theory (EMT) models [33]. In a series and parallel model, the heat transfer direction is assumed to be parallel and perpendicular to the material phases. However, all phases are mutually dispersed in the Maxwell and EMT models [33,34]. Table 1 summarizes the related equations of each model [16,35]. It should be noted that the pore distribution is not uniform in cement mortar; therefore, effective thermal conductivity measurement is complicated by the non-uniformity of pore distribution.

To calculate the effective thermal conductivity, the volume of pores should be determined in the first step. Pores are voids filled or emptied by trapped gas or fluids [36]. Therefore, the porosity in cement-based materials is the ratio of the volume of pores to the total volume of solid ($porosity(\%) = \frac{Volume\ of\ pores}{volume\ of\ solid\ included\ pores} * 100$) [37]. The pore system can be varied from nano millimeters up to hundreds of micrometers [38] and is classified as gel pores (up to 0.2 μm), capillary pores (0.2 μm–10 μm), and macro pores (more than 10 μm) [39]. Despite the importance of porosity, measurement is a challenging issue. There are various methods in prior literature for detecting porosity, such as gas adsorption [40], Mercury porosimeter [41], optical microscopy and image analysis [42], and x-ray tomography along the image processing [43–45].

After determining porosity, the volume of the solid phase of the mortar can be calculated. Also, the thermal conductivity of the void phase can be determined based on the thermal conductivity of air and water (it depends on the humidity situation of the sample). It should be noted that cement mortar is a multiscale material, and its solid phase comprises cement paste, sand (fine aggregate), and in some cases, fibers, admixture, and additives. The cement paste contains hydration products, gel, and capillary pores.

The previous literature showed that the thermal conductivity of cement paste ranges from 0.53 to 1.16 W/m.K [46]. In one study, Baghban et al. [24] evaluated the thermal conductivity of hydrated cement paste with different w/c ratios. They reported that the thermal conductivity of paste is 0.35–1.15 W/m.K for a wide range of w/c ratios depending on using additives and admixtures in different humidity levels. Also, another study proposed the thermal conductivity of 1 W/m.K for the hydrated cement paste and w/c ratios of 0.3–0.4 [46].
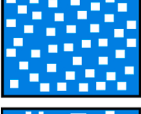
However, it is almost impossible to make a solid phase of mortar (cement paste and fine aggregate) without any porosity. Therefore, it is challenging to measure the thermal conductivity of the solid phase of mortar experimentally. Zhang et al. [21] proposed a helpful method to calculate the thermal conductivity of the solid phase of cement mortar. They used a back calculation by knowing the thermal conductivity of mortar and porosity volume as follows:

$$k_m = k_s \frac{2k_s + k_v - 2(k_s - k_v)p_v/(p_v + p_s)}{2k_s + k_v + (k_s - k_v)p_v/(p_v + p_s)} \tag{1}$$

Where, p_s and p_v are the volume of solids and voids, respectively and k_m, k_s, and k_v are the thermal conductivity of mortar (measured), solid, and void thermal conductivity, respectively.

Considering all these, previous literature showed that the total amount of void and the void distribution could affect the effective thermal conductivity of cement mortar [16]. For instance, the random distribution of pores was mentioned as the main reason for

Table 1
Models for effective thermal conductivity calculations.

Model	Effective thermal conductivity equation	Schematic structure
Series	$k_{eff} = \dfrac{1}{\frac{v_s}{k_s} + \frac{v_v}{k_v}}$	
Parallel	$k_{eff} = k_s v_s + k_v v_v$	
Maxwell	$k_{eff} = \dfrac{k_s v_s + k_v v_v \frac{3k_s}{2k_s + k_v}}{v_s + v_v \frac{3k_s}{2k_s + k_v}}$	
EMT	$v_s \dfrac{k_s - k_{eff}}{k_s + 2k_{eff}} + v_v \dfrac{k_v - k_{eff}}{k_v + 2k_{eff}} = 0$	

thermal conductivity variation in porous cement-based materials [47]. Therefore, the main drawback of predicted models is ignoring the air void distribution in the measured sample. However, there is no study to visualize the effective thermal conductivity of cement mortar based on void distribution. Therefore, this study aims to determine effective thermal conductivity through x-ray analysis which has not been considered previously.

For this reason, cement mortars with various proportions were cast. Then, their porosity and thermal conductivity were measured through an x-ray CT scanner and transient plane source method, respectively. The calculated thermal conductivity of the solid phase was imported to the VG studio software to determine the effective thermal conductivity of samples based on detected voids by a CT scanner.

2. Material and methods

2.1. Sample preparation

Industrial cement CEM I52.5 R from Norcem company was used as the binder. The NorStone company prepared the fine aggregate, and fresh portable water was applied. Then the materials were mixed at the mixer with the following proportions: 1) c:s ratio of 1:2 and w/c ratio of 0.42 (CM1:2), 2) c:s ratio of 1:3 and w/c ratio of 0.50 (CM1:3), and 3) c:s ratio of 1:4 and w/c ratio of 0.64 (CM1:4). The flow table test showed that the workability of these mixtures is similar and in the ranges of 190 ± 10 mm. The prisms with the dimension of $40 \times 40 \times 160$ mm^3 have been prepared and cured in water for 28 days.

2.2. Thermal conductivity

The prepared sample was cut in half ($40 \times 40 \times 80$ mm^3) and then analyzed by transient plane source (TPS) 2500 to measure its thermal conductivity. TPS is a transient method for measuring the thermal properties of the material. Two pieces of the specimen with a smooth surface are required for this. The sensor measured the increased temperature produced by the electric current. Before measurement, the samples were dried in the oven for 24 h at 105 °C. Equation (1) was applied to calculate the thermal conductivity of the solid phase of mortar.

2.3. X-ray computational tomography

Image acquisition and reconstruction are the two steps in a CT scanner to make a 3D image inside the cement mortar. In the first step, several 2D projections are acquired, and then the back-projection algorithm is used to reconstruct it as a 3D tomographic image [48–50]. In this study, a METROTOM 1500 G2 Scanner was applied to scan the sample, and the METROTOM OS 3.6.2.19227 was used
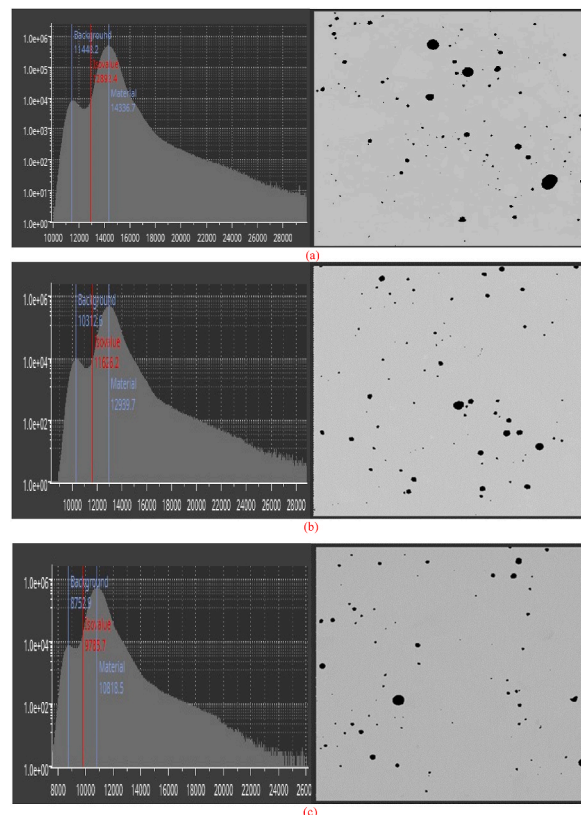

Fig. 1. Surface determination and segmentation for a) CM1:2, b) CM1:3, c) CM1:4. Gray value (x-axis) vs. Number of voxels (y-axis).

as the acquisition software. Three samples with dimensions of $40 \times 40 \times 80$ mm^3 were scanned with a voltage of 170 kV and a current of 426 μA.

Very important postprocessing of an image is segmentation to distinguish the void from the solid matrix. The method of segmentation is effective in the results of porosity. Prior literature reported different methods for the segmentation of an image, such as region-dependent techniques, boundary detection, and thresholding [51]. One of the common methods for segmentation in the void analysis is thresholding which divides the voxel into two different values (0 and 1 or black and white) [52]. Thresholding can be done using manual or automatic algorithms. The manual method is an observed-based method that visualizes the segmentation of a portion of CT scanner results. The automated algorithms are usually based on grayscale and histogram. This study used the software VG Studio max to analyze the images. Fig. 1 shows the surface determination for samples that segment solid and void phases.

There are two modes on VG Studio Max software for analyzing the effective thermal conductivity, i.e., experimental mode and tensors mode. In experimental mode, the inlet and outlet are defined while those are in different temperatures. Then the heat flux and void fraction are assigned for different sections. The results are based on the heat transfer simulation between the inlet and outlet. However, the tensor mode is based on calculating the tensorial effective thermal conductivity. In this study, both methods are applied.

3. Results and discussion

3.1. Void fraction

Cement mortar is a heterogenous material, and voids are distributed randomly. Based on the literature, the distribution of voids might influence effective thermal conductivity [4,16,25,53]. The void fraction of samples in different directions is shown in Fig. 2 (the voxel size of the acquisition image was 52 μm). Fig. 2 shows that the void fraction is not distributed homogenous and can be varied in each slice of the samples. However, the average value of detected macro porosity is 2.42%, 2.79%, and 3.22% for CM1.2, CM1.3, and CM1.4, respectively. The Root Means Square Error (RMSE) was applied to all three mixes for a more comprehensive analysis. The results showed that the highest error between the average macro porosity and the macro void fraction is related to the CM1:3 (RMSE = 1.35), CM1:2 (RMSE = 0.82), and CM 1:4 (RMSE = 0.64), respectively.

3.2. Simulation on experiment mode

The measurement results showed that the highest and lowest thermal conductivity belongs to the CM1:2 and CM1:4, respectively. Table 2 shows that the measured thermal conductivity of mixes with higher porosity is less than those with higher porosity. The outcome agrees with the literature's reported values [14]. The simulation of effective thermal conductivity based on the experiment mode of VG studio max was carried out as follows:

➢ The thermal conductivity of the solid phase was calculated by equation (1).
➢ The void phase's thermal conductivity (dry air's thermal conductivity) was assumed to be 0.024 W/m.K.
➢ The relative temperature difference on both sides is 1 K (Temperature differences between inlet and outlet)
➢ the boundary conditions are sealed
➢ The convection and radiations are neglected (Voids are smaller than 1 cm and measured at room temperature)
➢ the heat transfer was simulated in the direction of experimental measurement by TPS (parallel to the z axes) (Fig. 3a)
➢ The simulation continued until the convergence error was less than 1e-06 for the maximum number of iterations of 25000.
➢ The effective thermal conductivity for each slice was calculated using $k = \frac{\dot{q}}{\Delta x} \Delta T$

The measured thermal conductivity by TPS, detected porosity, calculated conductivity of solid phase, and effective thermal conductivity are summarized in Table 2. The heat flux and effective thermal conductivity in the experiment mode vary at different heights
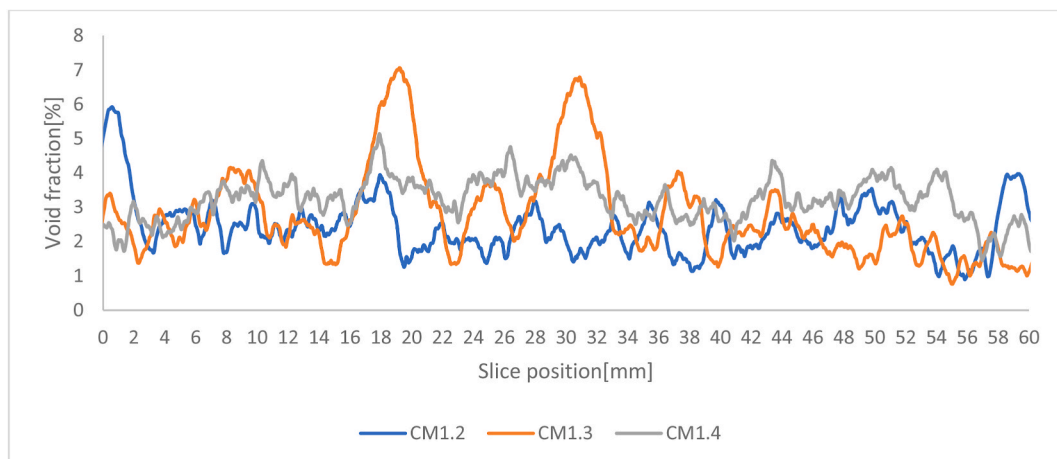

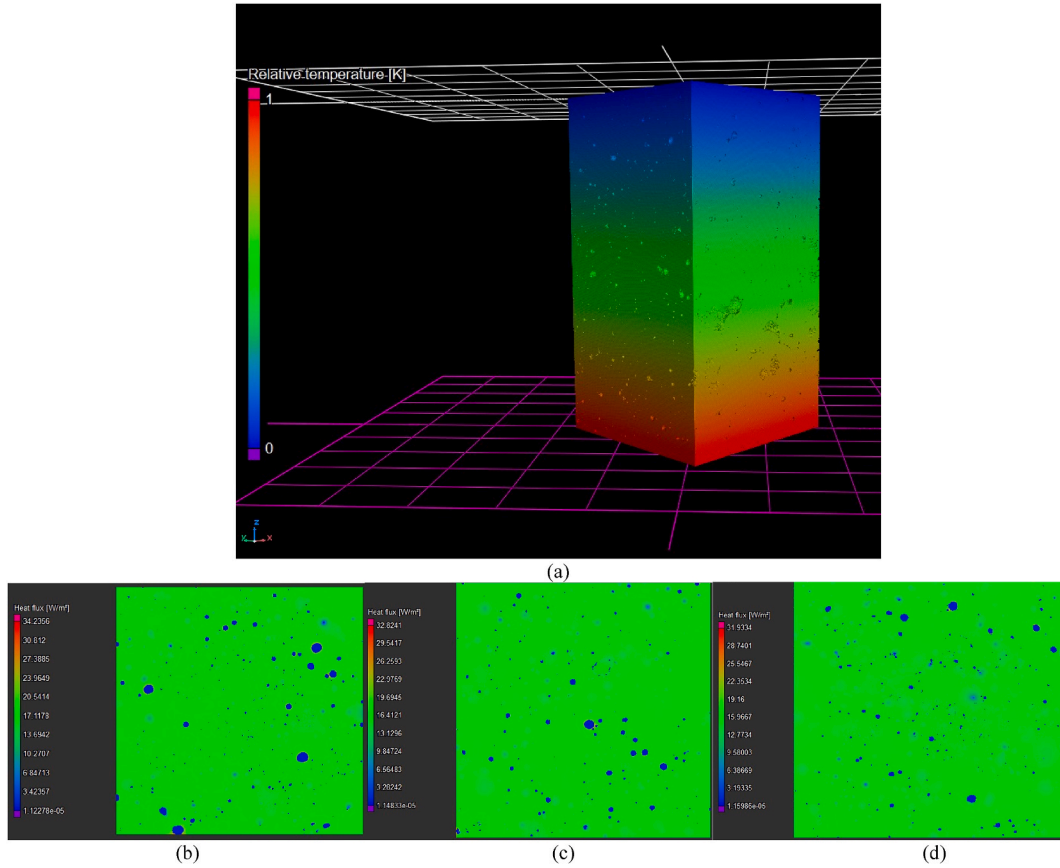**Fig. 2.** The void fraction of samples in different directions.

Fig. 3. a) Simulated the relative temperature when the heat transfer direction is parallel to the Z-axis, b) heat flux for CM1.2 at Z = 55, c) heat flux for CM1.3 at Z = 60, d) heat flux for CM1.4 at Z = 60.

Table 2
Thermal conductivity and porosity of cement mortar.

Sample ID	Measured thermal conductivity (W/m.K) by TPS	Porosity (%)	thermal conductivity of Solid (W/m.K)	Average effective thermal conductivity (W/m.K)
CM 1:2	1.13	2.42	1.17	0.97
CM 1:3	1.04	2.79	1.09	0.91
CM 1:4	1.00	3.22	1.05	0.87

(Fig. 3b, c, and 3d show the heat flux in one slice of samples). It can be attributed to the pore distribution in different sample locations (Fig. 4).

3.3. Simulation on tensors mode

The tensorial effective thermal conductivity was calculated in tensor mode, and the results are presented in this section. The effective thermal conductivity tensor for CM 1:2, CM 1:3, and CM 1:4 is shown in Equations (3)–(5). It should be noted that the VG studio software calculated the effective thermal conductivity tensor based on equation (2):

$$k_{ij}^{eff} = - \left[\varnothing_i^j \right] \frac{dL_j}{dT_j} \tag{2}$$

$$k_{eff}^{CM1.2} = \begin{bmatrix} 1.12116 & 0.000917029 & 0.000763844 \\ 0.000917029 & 1.12186 & 0.000440354 \\ 0.000763844 & 0.000440354 & 1.1222 \end{bmatrix} \left(\frac{W}{m.K} \right) \tag{3}$$

$$k_{eff}^{CM1.3} = \begin{bmatrix} 1.05162 & -0.0017839 & -0.000663 \\ -0.0017839 & 1.04878 & 0.000964955 \\ -0.000663 & 0.000964955 & 1.04911 \end{bmatrix} \left(\frac{W}{m.K} \right) \tag{4}$$
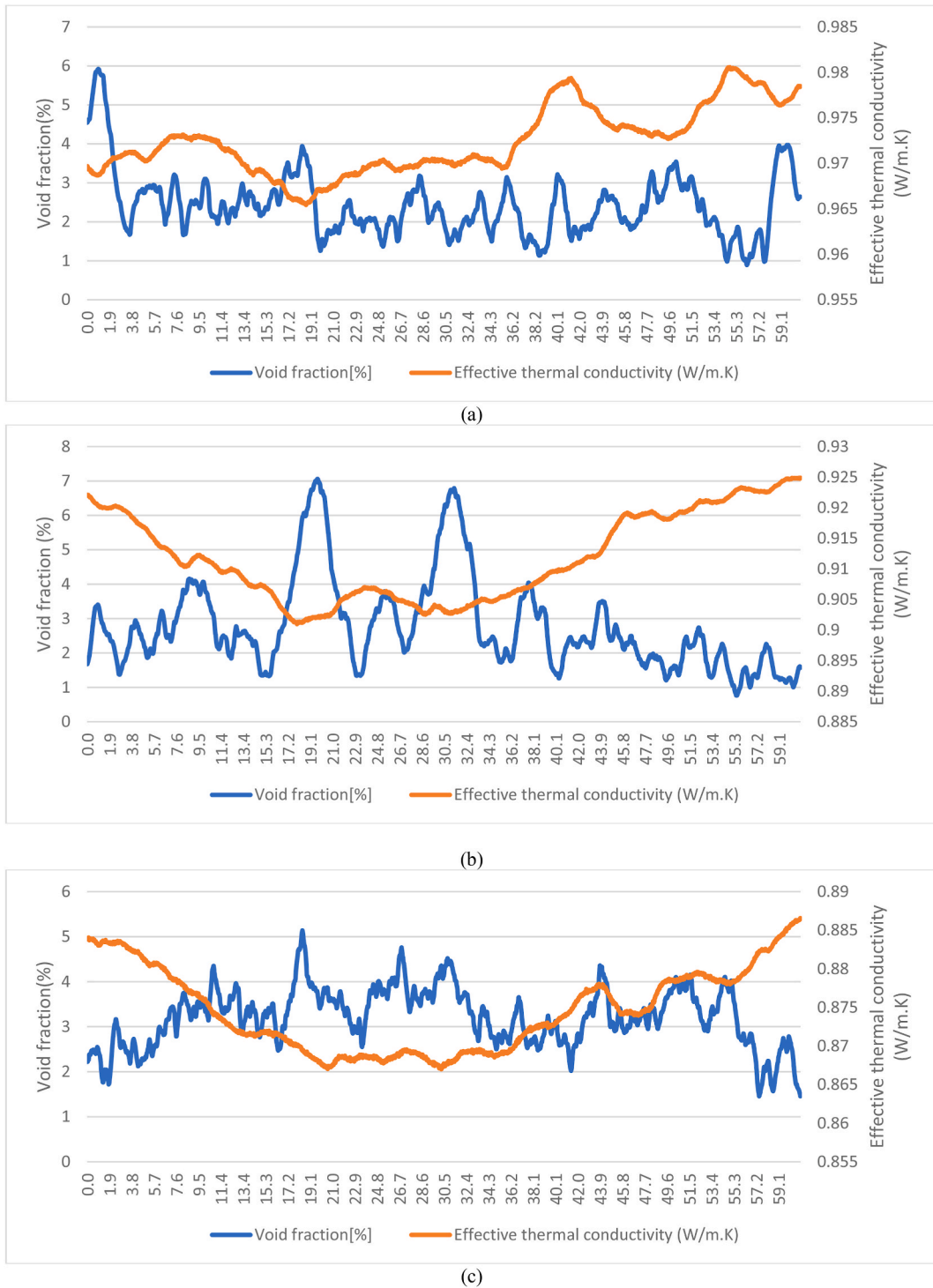
Fig. 4. The effective thermal conductivity vs. void fraction in different slice positions for a) CM 1:2, b) CM 1:3, and c) CM 1:4.

$$k_{eff}^{CM1.4} = \begin{bmatrix} 1.00589 & -0.00146744 & -0.000112094 \\ -0.00146744 & 1.00814 & -0.000246363 \\ -0.000112094 & -0.000246363 & 1.00799 \end{bmatrix} \left(\frac{W}{m.K}\right) \tag{5}$$

And the eigenvalues for each sample in different directions are as follows:

$$\lambda_1^{CM1.2} = 1.12043 \left(\frac{W}{m.K}\right), \lambda_2^{CM1.2} = 1.12161 \left(\frac{W}{m.K}\right), \lambda_3^{CM1.2} = 1.12318 \left(\frac{W}{m.K}\right) \tag{6}$$

$$\lambda_1^{CM1.3} = 1.04765 \left(\frac{W}{m.K}\right), \lambda_2^{CM1.3} = 1.04909 \left(\frac{W}{m.K}\right), \lambda_3^{CM1.3} = 1.05276 \left(\frac{W}{m.K}\right) \tag{7}$$

$$\lambda_1^{CM1.4} = 1.00515 \left(\frac{W}{m.K}\right), \lambda_2^{CM1.4} = 1.00797 \left(\frac{W}{m.K}\right), \lambda_3^{CM1.4} = 1.00889 \left(\frac{W}{m.K}\right) \tag{8}$$

And finally, the mean effective thermal conductivity for each sample can be mentioned as follows:

$$k_{eff,mean}^{CM1.2} = 1.12174 \left(\frac{W}{m.K}\right) \tag{9}$$

$$k_{eff,mean}^{CM1.3} = 1.04983 \left(\frac{W}{m.K}\right) \tag{10}$$

$$k_{eff,mean}^{CM14} = 1.00734 \left(\frac{W}{m.K}\right) \tag{11}$$

The visualization of mean effective thermal conductivity for different samples is shown in Fig. 5.

The measured results were compared with CT scanner output in experiment and tensors modes. Fig. 6 shows that the measured results agree with the experiment mode in the z-direction (TPS sensors were in parallel with the x-y plane and measured values are in the z-direction).

4. Conclusion

The thermal conductivity of cement mortar is an influential parameter on heat transfer and energy consumption. Since cement mortar is a heterogenous material, the effective thermal conductivity is a function of both the solid and void phases. Despite the available literature, this study detected the voids content and distribution in the mortar with different mixed proportions using an x-ray CT scanner. The results showed that the effective thermal conductivity could vary in positions and samples due to the percentages of void content and void distribution in the sample. Thermal conductivity of CM1:3 and CM1:4 decreased by 8% and 11.5% compared to the CM1:2. Moreover, the percentage of pore content (larger than 52 μm) at CM1:3 and CM1:4 increased by 15% and 33% compared to the CM1:2. Despite the variation in effective thermal conductivity in different locations, the mean values of simulations are in the excellent agreement with the measured thermal conductivity by TPS. For instance, the difference between the mean effective thermal conductivity in tensors mode and TPS measurement is less than 1% for all samples. One of the main reasons for the high simulation accuracy of VG Studio Max software is the solid-phase thermal conductivity value calculated from the measured value. It needs to be input into the software, increasing the accuracy of the prediction results but making the practical application more difficult. Other
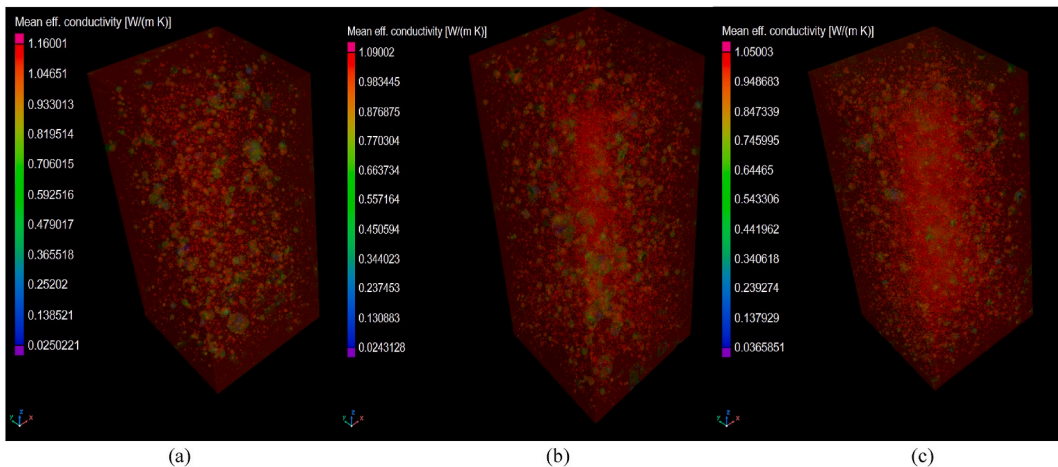

Fig. 5. The mean effective thermal conductivity for a) CM 1:2, b) CM 1:3, and c) CM 1:4.
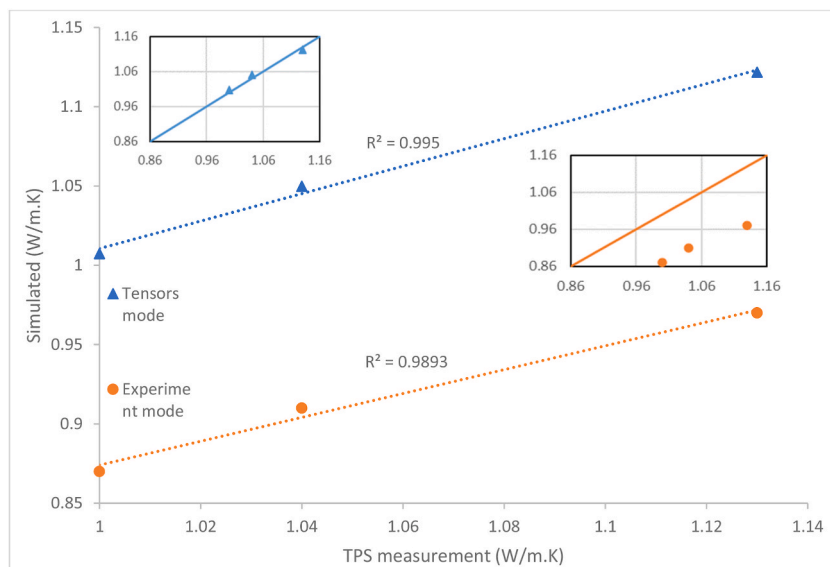
Fig. 6. The measured thermal conductivity vs. the simulated effective thermal conductivity.

solid-phase thermal conductivity mentioned in the literature should be used for future work to prove the simulation results.

Author statement

1. Iman Asadi: Conceptualization, Methodology, Software, Formal analysis, Investigation, Writing - Original Draft.
2. Guomin Ji, Resources, Supervision.
3. Mohammad Hajmohammadian Baghban: Review & Editing.

Declaration of competing interest

The authors declare that they have no known competing financial interests or personal relationships that could have appeared to influence the work reported in this paper.

Data availability

No data was used for the research described in the article.

Acknowledgment

References

[1] I. Flores-Colen, J.d. Brito, Renders, in: Materials for Construction and Civil Engineering, Springer, 2015, pp. 53–122.
[2] M.C. Gonçalves, F. Margarido, Materials for Construction and Civil Engineering, Springer, Cham, Switzerland, 2015.
[3] J.A. Pulido-Arcas, V. Flores-Alés, A. Pérez-Fargallo, Coating mortars with improved physical properties, economic cost, and carbon footprint, Case Stud. Constr. Mater. 16 (2022), e01095.
[4] F. Batool, N.N. Prasad, V. Bindiganavile, Statistical modeling of thermal conductivity for cement-based foam, J. Build. Eng. 19 (2018) 449–458.
[5] A. Adesina, Recent advances in the concrete industry to reduce its carbon dioxide emissions, Environ. Chall. 1 (2020), 100004.
[6] I. Asadi, et al., Evaluating the time lag and decrement factor of mortar and concrete containing OPBC as an agricultural by-product lightweight aggregate, Case Stud. Therm. Eng. (2022), 102609.
[7] L.L. Sparks, NASA STI/Recon Technical Report N, Thermal Conductivity of a Concrete Mortar from 95 K to 320 K, vol. 82, 1981, 24396.
[8] EN 998-1:2016: Specification for Mortar for Masonry – Part 1: Rendering and Plastering Mortar, BSI, London, UK, 2016.
[9] I. Tavman, Effective thermal conductivity of granular porous materials, Int. Commun. Heat Mass Tran. 23 (2) (1996) 169–176.
[10] A.V. Luikov, Heat and mass transfer in capillary-porous bodies, in: Advances in Heat Transfer, Elsevier, 1964, pp. 123–184.
[11] W. Woodside, Calculation of the thermal conductivity of porous media, Can. J. Phys. 36 (7) (1958) 815–823.
[12] C. Wang, et al., Thermal characteristics and recoverability of early-age mortar consisting of a flame retardant Mg (OH) 2, J. Build. Eng. 57 (2022), 104897.
[13] I. Asadi, et al., Thermal conductivity of concrete–A review, J. Build. Eng. 20 (2018) 81–93.
[14] P. Shafigh, et al., Thermal properties of cement mortar with different mix proportions, Mater. Construcción 70 (339) (2020) e224-e224.
[15] H.R. Talebi, et al., Investigation of thermal properties of normal weight concrete for different strength classes, J. Environ. Treat. Tech 8 (3) (2020) 908–914.
[16] F. Batool, M.M. Rafi, V. Bindiganavile, Microstructure and thermal conductivity of cement-based foam: a review, J. Build. Eng. 20 (2018) 696–704.
[17] B.-H. Woo, et al., Estimation of the thermal conductivity of cement composites using bayesian statistical approach, Compos. B Eng. (2022), 110073.

[18] M.H. Baghban, M. Kioumarsi, S. Grammatikos, Prediction models for thermal conductivity of cement based composites, Nord. Concr. Res. 58 (1) (2018) 163–171.
[19] T. Wu, I. Temizer, P. Wriggers, Computational thermal homogenization of concrete, Cement Concr. Compos. 35 (1) (2013) 59–70.
[20] M. Mohammad, et al., Properties and microstructure distribution of high-performance thermal insulation concrete, Materials 13 (9) (2020) 2091.
[21] W. Zhang, et al., Mesoscale model for thermal conductivity of concrete, Construct. Build. Mater. 98 (2015) 8–16.
[22] Y. Du, Y. Ge, Multiphase model for predicting the thermal conductivity of cement paste and its applications, Materials 14 (16) (2021) 4525.
[23] N. Balaji, M. Mani, B.V. Reddy, Discerning heat transfer in building materials, Energy Proc. 54 (2014) 654–668.
[24] M. Hajmohammadian Baghban, P.J. Hovde, S. Jacobsen, Analytical and experimental study on thermal conductivity of hardened cement pastes, Mater. Struct. 46 (9) (2013) 1537–1546.
[25] F. Batool, V. Bindiganavile, Evaluation of thermal conductivity of cement-based foam reinforced with polypropylene fibers, Mater. Struct. 53 (1) (2020) 1–16.
[26] F. Batool, V. Bindiganavile, Microstructural parameters of fiber reinforced cement-based foam and their influence on compressive and thermal properties, J. Build. Eng. 31 (2020), 101320.
[27] F. Batool, M.S. Khan, V. Bindiganavile, Characterization of 3D microstructure, thermal conductivity, and heat flow of cement-based foam using imaging technique, Front. Struct. Civ. Eng. 15 (3) (2021) 643–651.
[28] H. Russell, Principles of heat flow in porous insulators, J. Am. Ceram. Soc. 18 (1-12) (1935) 1–5.
[29] R. Pande, V. Kumar, D. Chaudhary, Thermal conduction in a homogeneous two-phase system, Pramana 22 (1) (1984) 63–70.
[30] J.C. Maxwell, A Treatise on Electricity and Magnetism, vol. 1, Clarendon press, 1873.
[31] D. Chaudhary, R. Bhandari, Heat transfer through a three-phase porous medium, J. Phys. Appl. Phys. 1 (6) (1968) 815.
[32] J. Wyrwał, A. Marynowicz, J. Świrska, Effective thermal conductivity of porous building materials–analysis and verification, Bauphysik 30 (6) (2008) 431–433.
[33] J. Wang, et al., A new structural model of effective thermal conductivity for heterogeneous materials with co-continuous phases, Int. J. Heat Mass Tran. 51 (9–10) (2008) 2389–2397.
[34] A. Karaki, et al., Theoretical and computational modeling of thermal properties of lightweight concrete, Case Stud. Therm. Eng. 28 (2021), 101683.
[35] J. Wang, et al., A new approach to modelling the effective thermal conductivity of heterogeneous materials, Int. J. Heat Mass Tran. 49 (17–18) (2006) 3075–3083.
[36] M. Allaby, A Dictionary of Geology and Earth Sciences, Oxford University Press, 2013.
[37] V.A. Jaques, et al., Review of porosity uncertainty estimation methods in computed tomography dataset, Meas. Sci. Technol. 32 (12) (2021), 122001.
[38] R.A. Cook, K.C. Hover, Mercury porosimetry of hardened cement pastes, Cement Concr. Res. 29 (6) (1999) 933–943.
[39] P. Pipilikaki, M. Beazi-Katsioti, The assessment of porosity and pore size distribution of limestone Portland cement pastes, Construct. Build. Mater. 23 (5) (2009) 1966–1970.
[40] Y. Aono, et al., Nano-structural changes of CSH in hardened cement paste during drying at 50 C, J. Adv. Concr. Technol. 5 (3) (2007) 313–323.
[41] S. Diamond, Mercury porosimetry: an inappropriate method for the measurement of pore size distributions in cement-based materials, Cement Concr. Res. 30 (10) (2000) 1517–1525.
[42] E.K. Nambiar, K. Ramamurthy, Air-void characterisation of foam concrete, Cement Concr. Res. 37 (2) (2007) 221–230.
[43] S. Stock, Recent advances in X-ray microtomography applied to materials, Int. Mater. Rev. 53 (3) (2008) 129–181.
[44] N. Bossa, et al., Micro-and nano-X-ray computed-tomography: a step forward in the characterization of the pore network of a leached cement paste, Cement Concr. Res. 67 (2015) 138–147.
[45] J. Yoon, et al., Characterization of porous cementitious materials using microscopic image processing and X-ray CT analysis, Materials 13 (14) (2020) 3105.
[46] D. Bentz, Transient plane source measurements of the thermal properties of hydrating cement pastes, Mater. Struct. 40 (10) (2007) 1073–1080.
[47] J. Chen, et al., Analysis of thermal conductivity of porous concrete using laboratory measurements and microstructure models, Construct. Build. Mater. 218 (2019) 90–98.
[48] P.J. Withers, et al., X-ray computed tomography, Nat. Rev.Methods Prim. 1 (1) (2021) 1–21.
[49] E.N. Landis, D.T. Keane, X-ray microtomography, Mater. Char. 61 (12) (2010) 1305–1316.
[50] I. Asadi, et al., Macro pore content in wet-sprayed concrete characterized by CT scanning, in: Fib International Congress, 2022 (Oslo).
[51] S.U. Lee, S.Y. Chung, R.H. Park, A comparative performance study of several global thresholding techniques for segmentation, Comput. Vis. Graph Image Process 52 (2) (1990) 171–190.
[52] I. Asadi, P.E. Endrerud, S. Jacobsen, X-ray tomography to characterize the air-void system of hardened concrete with varying sample size, in: fib International Congress, 2022.
[53] F. Batool, V. Bindiganavile, Air-void size distribution of cement based foam and its effect on thermal conductivity, Construct. Build. Mater. 149 (2017) 17–28.